Impacts of large scale integration of wind power on power system small-signal stability

José L. Rueda István Erlich
Institute of Electric Power Systems
University Duisburg-Essen
Duisburg, Germany
E-mail: jose.rueda@uni-duisburg-essen.de, istvan.erlich@uni-due.de

Abstract—**In this paper, based on a small-size power system, a deterministic assessment on the impact of wind power on power system small-signal stability is first thoroughly discussed. Next, a realistic weak wind-hydro-thermal (WHT) power system is used to ascertain if the indicative findings of the preliminary work can be confirmed by a large scale case study. Subsequently, Monte Carlo based probabilistic eigenanalysis is implemented on the weak WHT system in order to further corroborate the findings drawn from the deterministic studies. It was found out that large wind power integration can have positive or negative impacts on system damping depending on the location of the wind power plant, the amount of the conventional generation replaced by wind power and the stress level of the power system.**

Keywords-Small-signal stability, eigenanalysis, wind power, doubly-fed Generator

I. INTRODUCTION

Outstandingly, wind power capacity in North America and in Europe has grown at a rate of 20% to 40% per year over the past decade. Therefore, extrapolating the current trend into the future, it is easy to foresee installed wind capacities exceeding 50 % of the overall capacity in some countries in the not too distant future [1]. A reason for this fact is the incentive policies adopted by several countries to support renewable energy development. For instance, the pioneer countries with the most installed wind capacity (Germany, Spain and Denmark) promoted some sort of feed-in tariff, which established a mandatory purchase price for wind energy for a fixed period of time. This ensured a stable long-term policy environment and encouraged significant investments in wind power plants [2]. Speaking in terms of energy penetration levels (i.e. the ratio of the wind energy delivered divided by the total energy delivered), the actual penetration levels in Germany, Spain and Denmark are above 8%, 6% and 20% respectively [3].

Nearly all wind generation systems currently in use employ either one of the following schemes: i) The directly grid coupled squirrel-cage induction generator: it corresponds to the constant speed wind turbine, which is commonly used in old wind power plants. The wind turbine rotor is coupled to the rotor through a gearbox; ii) The doubly-fed generator (DFG): the rotor winding is fed using a back-to-back voltage source converter. The wind turbine rotor is coupled to the rotor through a gearbox; and ii) The direct drive synchronous generator: it is grid coupled through a power electronic converter. No gearbox is needed if the synchronous generator is a low speed multipole generator. The main differences between the three schemes are the generating system and the way in which the aerodynamic efficiency of the rotor is limited during wind speed variations [4], [5].

From a literature survey, it can be found that each of the aforesaid wind generating systems has its own benefits and drawbacks. Moreover, it is worth to mention that almost all newer larger wind generating systems (rated up to the 5 MW class) being produced are variable speed systems which use DFGs with full-scale converter [6]. DFG-based systems possess important characteristics such as high transfer efficiency of energy, low investment and flexible controls. Additionally, DFGs have some reactive power control capabilities and other advantages [7]. Many publications on the topic of wind generation system modeling can be found in the literature. The presented models have been extensively tested and can be used in power system steady state and dynamic simulations. Thus, the research presented in this paper focuses on the DFG-based generation system and uses the model presented in [16] whose behavior resembles that of the system with full-scale converter.

With increasing wind power generation, interest to fully understand and quantify the impact of this development on the performance of the interconnected systems has also grown. While individual onshore wind units in the past were only required to maintain a prescribed power factor range at the point of interconnection, now transmission system operators (TSOs) are putting more wide-ranging conditions. Some TSOs have issued grid codes spelling out a range of operational requirements, which wind farms need to fulfill upon connection to the grid. These include low voltage fault ride-through capability and voltage support following grid faults. Requirements concerning additional ancillary services are also likely to follow. It should also be borne in mind that the control systems which modern wind turbines employ are characterized by fast response time and thus open up additional, unconventional options to help meet these requirements [8]. The inherent differences between conventional generating systems and wind power generating systems are reflected in a

different interaction with the power system. Therefore, a number of studies have dealt with various aspects related to local and system wide impacts of wind power. Local impacts occur in the electrical vicinity of a wind power plant [9]. Hence, power flow analysis, the study of protection schemes and power quality have already been studied extensively [10]. On the other hand, system wide impacts affect the behavior of a power system as a whole and are strongly related to the penetration level in the system [9]. The impacts on system balancing (frequency control and dispatch of conventional generating units), voltage stability and transient stability are among the main aspects analyzed in studies related to large scale wind power integration [11].

Recently, the impact of large scale wind power integration on power system small-signal stability has become a topic of increased interest and discussion. Although it has been pointed out that wind generation systems do not themselves lead to power system oscillations [5], the location of wind power plants and the variability of wind power plants' output may indirectly involve positive or negative impacts on damping of power system oscillations [12]. Only few research works addressing this problem have been reported [13]. However, despite the relevance of the adopted approaches, the results underscore the potential need of further research for better understanding of the main factors influencing the impact of large scale wind power integration on power system small-signal stability. With this aim in mind, this paper provides an attempt in this direction by ascertaining, through linearization-based eigenalysis, time domain simulations, and probabilistic eigenanalysis, how different wind power integration levels and wind power plant locations affects the system small-signal stability performance.

The outline of the paper is as follows: Section II introduces some theoretical background about linearization-based eigenanalysis, probabilistic eigenanalysis, and DFG modeling. In Section III, test cases are developed and evaluated. Finally, conclusions are summarized in Section IV.

II. BACKGROUND THEORY

A. Linearization-based eigenanalysis

To analyse the power system small-signal stability mathematically, the disturbances can be considered to be small in magnitude in order to linearize the set of non-linear-algebraic equations (1)-(3) that is widely used to represent the dynamics of the system [14]:

$$\dot{\mathbf{x}}_s = \mathbf{f}(\mathbf{x}_s, \mathbf{x}_a, \mathbf{u}), \quad \mathbf{x}_s \in \mathbf{R}^n \quad \mathbf{u} \in \mathbf{R}^p \tag{1}$$

$$0 = \mathbf{g}(\mathbf{x}_s, \mathbf{x}_a, \mathbf{u}), \quad \mathbf{x}_a \in \mathbf{R}^m \tag{2}$$

$$\mathbf{y} = \mathbf{h}(\mathbf{x}_s, \mathbf{x}_a), \quad \mathbf{y} \in \mathbf{R}^q \tag{3}$$

where (1) models differential equations of device dynamics, $\mathbf{x_s}$ represents state variables, $\mathbf{x_a}$ represents algebraic variables (e.g. magnitude and phase of node voltages), $\mathbf{u}$ represents vector of input variables and $\mathbf{y}$ denotes vector of output variables. Assuming that input control variables do not directly affect the outputs, the linear representation of (1)-(3) around a system operating point is expressed as follows:

$$\Delta\dot{\mathbf{x}}_s = \mathbf{A}_{11}\Delta\mathbf{x}_s + \mathbf{A}_{12}\Delta\mathbf{x}_a + \mathbf{B}_1\Delta\mathbf{u} \tag{4}$$

$$0 = \mathbf{A}_{21}\Delta\mathbf{x}_s + \mathbf{A}_{22}\Delta\mathbf{x}_a + \mathbf{B}_2\Delta\mathbf{u} \tag{5}$$

$$\Delta\mathbf{y} = \mathbf{C}_1\Delta\mathbf{x}_s + \mathbf{C}_2\Delta\mathbf{x}_a \tag{6}$$

Without algebraic variables the set of equations (4)-(6) can be reduced to the following form:

$$\Delta\dot{\mathbf{x}}_s = \mathbf{A}\Delta\mathbf{x}_s + \mathbf{B}\Delta\mathbf{u} \tag{7}$$

$$\Delta\mathbf{y} = \mathbf{C}\Delta\mathbf{x}_s \tag{8}$$

where,

$$\mathbf{A} = \mathbf{A}_{11} - \mathbf{A}_{12}\mathbf{A}_{22}^{-1}\mathbf{A}_{21} \tag{9}$$

$$\mathbf{B} = \mathbf{B}_1 - \mathbf{A}_{12}\mathbf{A}_{22}^{-1}\mathbf{B}_2 \tag{10}$$

$$\mathbf{C} = \mathbf{C}_1 - \mathbf{C}_2\mathbf{A}_{22}^{-1}\mathbf{A}_{21} \tag{11}$$

The eigenvalues of the state matrix $\mathbf{A}$ (i.e. λ_i, i=1…n) determine the time domain response of the system to small perturbations and therefore provides valuable information regarding the stability characteristics of the system. The critical eigenvalues are characterized by being complex (also denominated swing modes or oscillatory modes) and by being located near the imaginary axis of the complex plane. For a particular eigenvalue $\lambda_i = \alpha_i + j\omega_i$, the frequency of the oscillation is given by $\omega_i/2\pi$, and the damping ratio ζ_i is given by:

$$\zeta_i = -\alpha_i \Big/ \sqrt{\alpha_i^2 + \omega_i^2} \tag{12}$$

The mode shape associated to each critical eigenvalue helps to distinguish the various types of oscillation. The phase angle of speed elements in the right eigenvector belonging to a critical mode indicates the phase contribution of each state variable to that mode. Moreover, a speed participation factor indicates the relative contribution of each state variable to a certain mode. Thus, high speed participation factors and phase angle differences in the order of 180º indicate oscillation between groups of generators. Besides, the location of the generators in the power system determines the oscillation type [14].

B. Probabilistic eigenanalysis

The framework of the Monte-Carlo-based (MC) probabilistic eigenanalysis approach that is employed in this paper is sketched schematically in Fig. 1. The procedure begins with the definition of the probabilistic models of system input variables, the actual system model for power system dynamic analysis, and the requirements imposed on the system by the small-signal stability constraint in order to guarantee secure operation. Next, all components of the input nodal vector are obtained through random sampling of generation and load variables according to their probability distribution function models (PDFs). For this purpose, discrete PDFs are used to model the change of generator dispatches whereas the multivariate normal PDF is employed to represent nodal demand uncertainties around a specific loading condition. Each trial input vector defines an operating state which is determined by power flow calculation. Viable operating states that fulfill steady state voltage limits, thermal overloading of transmission

elements, and maintain the generation units operating within their limits are then selected. Next, the system small-signal stability performance is evaluated via linearization-based eigenanalysis for each viable operating state. Here, critical modes, their associated frequency, ζ, right eigenvectors and left eigenvectors are calculated. An eigenvalue tracking procedure based on modal parameters is also applied at this stage to ensure proper storage of linearization-based eigenanalysis information and to ensure proper statistical evaluation of computed critical mode parameters. Besides, sequential estimation of statistical relative error is applied in probabilistic eigenanalysis in order to ensure a high degree of confidence. Thereafter, the resulting mode frequency and damping statistics are defined in terms of their respective mean values and standard deviations. Also, the probabilistic index R_{Inst} is calculated to assess the instability risk due to negatively damped or lowly damped oscillatory modes (OMs). Based on a defined ζ threshold (e.g. ζ_i >5%), the R_{Inst} index is calculated accounting the cumulative probability distribution function (CPDF) associated to each critical mode ζ as follows:

$$R_{\text{Inst}} = \begin{cases} \text{OM}_{\zeta\text{-Neg}} = \text{P}(\zeta_i < 0) \\ \text{OM}_{\zeta\text{-Poor}} = \text{P}(0 \le \zeta_i < 5\%) \;\; i = 1, \cdots, M_C \\ \text{OM}_{\zeta\text{-Damp}} = \text{P}(\zeta_i \ge 5\%) \end{cases} \quad (13)$$

where $\text{OM}_{\zeta\text{-Neg}}$ indicates the probability of instability due to negatively damped OM, $\text{OM}_{\zeta\text{-Poor}}$ indicates the probability associated to poorly damped OM, and $\text{OM}_{\zeta\text{-Damp}}$ indicates the probability associated to well damped OM. M_C is the number of critical modes, and P(.) denotes cumulative probability.

C. DFG modeling

As is well known, the rotor terminals of a DFG are fed with a symmetrical three-phase voltage of variable frequency and amplitude fed through a voltage source converter usually equipped with IGBT based power electronic circuitry [16]. The basic topology including its control system is shown in Fig. 2. As a general approach, the space-phasor coordinates with orthogonal direct (d) and quadrature (q) axis is used. The choice of the stator voltage as the reference frame enables the decoupled control of P (d control channel) and Q (q control channel). The two complex (i.e. complex in terms of space-phasor representation) voltage differential equations, one each for the stator and rotor circuits, together with the equation of motion represent the full set of mathematical relationships that describe the dynamic behavior of the machine [17]. Then, by setting the derivative of the stator flux linkage with respect to time to zero, the quasi stationary model of the machine is obtained [8]. A complete model of the DFIG also includes models of the real and reactive power control together with speed and pitch angle control. Damping control is also embedded into the speed control structure. However, it is not detailed in this paper but considered in simulations. The structures of both the line side controller (LSC) and the rotor side controller (RSC) are given in Fig. 3 and Fig. 4, respectively. The two figures summarize the models of the core functionalities of the systems, which are of relevance for stability studies. The structures as presented here reproduce neither any eventual blocking of the converters nor crowbar activation during grid faults. The air gap torque of the machine is also assumed to remain constant. The voltage controller in Fig. 4 maintains a deadband of ±5 % to preclude controller action until the voltage exits this limit [8].

A complete model of a wind power plant with a high number of wind generators may lead to excessive calculation time, especially for stability studies. Thus, several studies have shown that it is not necessary to represent the individual wind generators in a wind power plant [5]. Representation of a wind power plant by a single generator can be achieved by the following assumptions [14]:

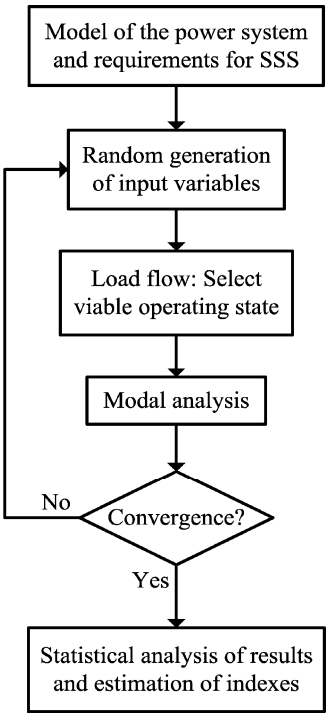

Figure 1. Monte Carlo-based probabilistic eigenanalysis

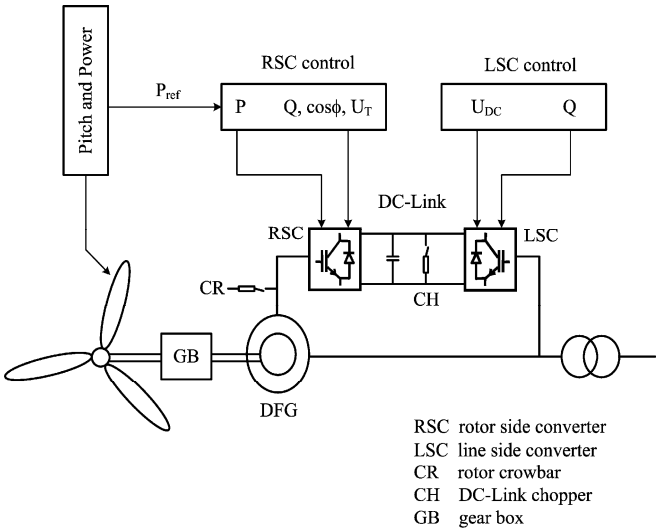

Figure 2. DFG-based wind generation system

- Equivalent generator model including the detailed controller models same as individual but with MVA rating equal n times individual generator rating.
- Equivalent generator step-up transformer same as individual but with MVA rating equal to n times individual transformer rating.
- Interconnection substation modeled as is.
- Equivalent collector system modeled as a single line with charging capacitance equal to total of the individual collector lines and with series R and X adjusted to give approximately the same P and Q output at the interconnection substation at rated generator output as the full system.

These assumptions imply that internal network and any internal interactions within the wind power plant are neglected [5]. Also, wind-speeds and mechanical speeds are assumed to be almost the same for each wind turbine [18].

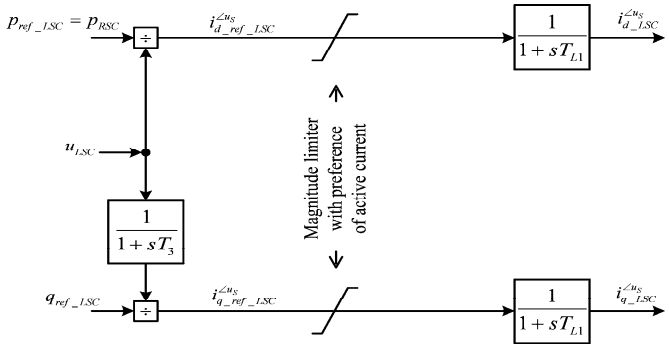

Figure 3. LSC model

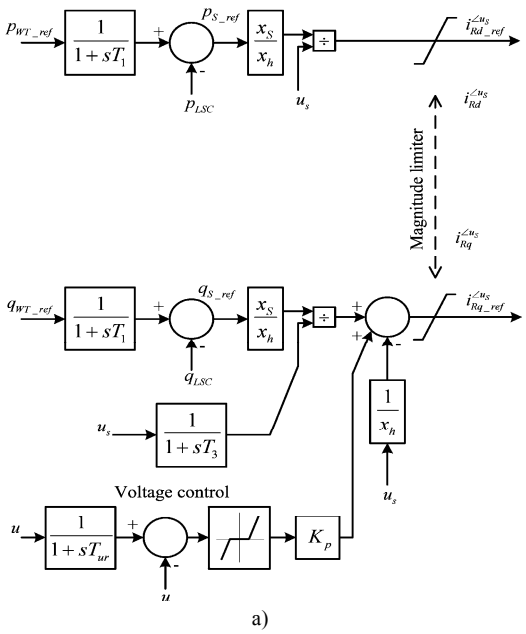

a)

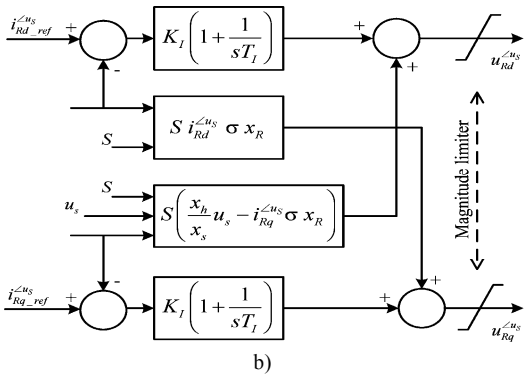

b)

Figure 4. RSC model: a) Structure for generating rotor current reference values, b) Rotor current control

III. TEST CASES AND DISCUSSION

Numerical experiments were performed on a HP Pavilion dv3 PC with Intel (R) Core (TM) 2 CPU, 2.2 GHz processing speed, and 4 GB RAM. The modeling, load flow, and linearization-based eigenanalysis were accomplished by several routines written in Matlab which utilize some modified functions of the Power System Dynamics simulation package (PSD) [19].

A. Small-size power system – deterministic assessment

In this study, the two area-four machine (TAFM) power system presented in [17] has been modified to assess the impact of a DFG-based wind power plant on small-signal stability. The single line diagram is depicted in Fig. 5. This system exhibits three OMs: one inter-area mode, in which the generating units in Area 1 oscillate against those in Area 2, and two local modes, one in each area, associated with the oscillations of the generating units within each area. The parameters of thermal generators G1 to G4, transformers and transmission lines are derived from those of the WHT system given in [20]. The rated power of each synchronous generator is 247 MVA whereas the rated power of the wind power plant is 750 MVA. This corresponds to the output of 150 DFG-based wind generators, each with a nominal capacity of about 5 MVA. A single equivalent model was used to represent all individual units within the wind power plant in order to avoid increasing computation time, and it is connected to the system using a typical layout of an offshore wind power plant as shown in Fig. 6. Synchronous generators are modeled using the fifth order model. Governors and excitation systems are modeled using different IEEE standard models [17].

In common practice, wind power is dispatched on a priority basis irrespective of its merit order [8]. This may involve a shift of generation profiles and power flows in the transmission network, which may have significant impact on small-signal stability. Hence, the TAFM system was studied for different scenarios generated from a highly loaded condition and corresponding to different power generation dispatches of conventional synchronous machines and wind power plants in order to create different wind power generation levels. Here, each power output from the wind power plant will correspond to the power available for a given wind speed. Each scenario will define an operating state which is determined through load

flow calculation. Next, linearization-based eigenanalysis will be performed in each scenario. This will help in explaining the sensitivities of the OMs with respect to the levels of wind power generation. Besides, since power system oscillations are caused by the working principle of synchronous generators and considering that power system dynamic behavior is highly nonlinear, time domain simulations will be useful to validate results from linearization-based eigenanalysis. The initial scenario comprises to a total load demand of 2734 MW, with 967 MW and 1767 MW corresponding to the loads at buses 4 and 14 respectively, 2652.5 MW of conventional generation power and 215.7 MW of wind power. From this scenario, two separate wind power plant locations are considered in order to investigate the effect of a wind power plant located within the same highly loaded area (Area 2) or with a wind power plant located far from that area (Area 1):

- Wind power plant connected to bus 120: Wind generation increase gradually whereas conventional generation in i) in G3 (Case 1), or ii) in G2 and G3 (Case 2) reduce.
- Wind power plant connected to bus 20: Wind generation increase gradually whereas conventional generation in G3 and G4 reduce (Case 3).

Case1 and Case 2

In Case 1, G3 generation was replaced gradually by wind generation while keeping unaltered the power transfer between areas. Fig. 7 shows the root loci for the inter-area mode and the two local modes. The circle markers represent the initial scenario and the square markers the final scenario (85 % of G3 generation replaced by wind generation). The upward-pointing triangle marker represents the scenario when G3 was fully replaced by wind generation. It can be seen that the damping of the inter-area mode and the Area 2 local mode increase whereas the damping of the Area 1 local mode is not significantly affected. This probably means that wind power does not affect local oscillations in distant areas.

Additionally, the Area 2 local mode no longer exists and the inter-area mode path changes when G3 was fully replaced by wind generation. These changes arise from the fact that synchronous generator G3 (which is involved in both types of oscillatory modes) is replaced by the wind power plant. Besides, the changes in modal characteristics can be due to the fact that DFG does not interface with the network through an internal angle as a synchronous machine does. This causes the absence of mechanical states associated to G3 (speed and angle) from the right eigenvector associated to each corresponding eigenvalue. This situation is depicted in Fig. 8 and Fig. 9, when comparing the mode shapes and participation factors for inter-area mode.

In Case 2, G2 and G3 generation was replaced gradually by wind generation. The movement of the OMs in the complex plane is shown in Fig, 10. Again, the circle markers represent the initial scenario and the square markers the final scenario (50 % of G2 and G3 generation replaced by wind generation). It can be observed that the three OMs exhibit a small increase of damping. Further, the changes in the three modes arise from the fact that the power generation from synchronous generators G2 and G3 (which are involved in the three types of oscillatory modes) is partially replaced by wind power generation, and because of power transfers from Area 1 to Area 2 have decreased (G2 output power level was diminished and replaced by wind power). In this case, the power system is less stressed (conventional generators operating far from their limits and less power transfers between the two areas). Thus, the wind power plant appears to contribute to damping enhancement when increasing wind power generation helps in reducing the power system stress level.

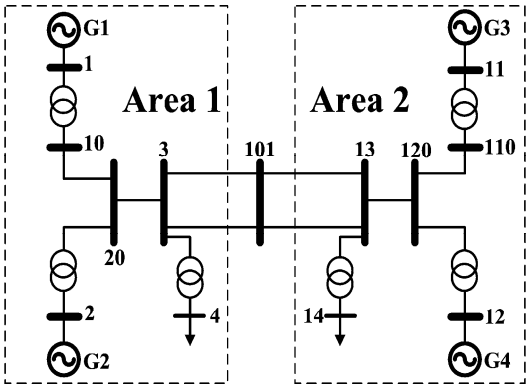

Figure 5. Single-line diagram of the TAFM system

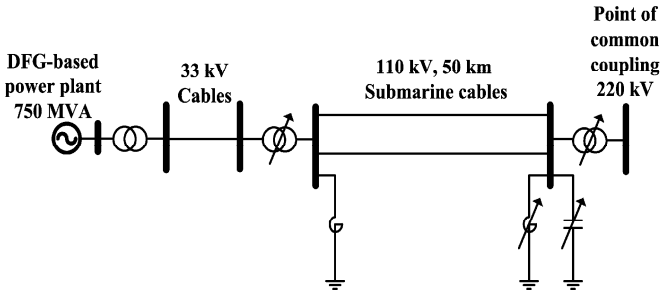

Figure 6. Connection of an offshore wind power plant to the grid

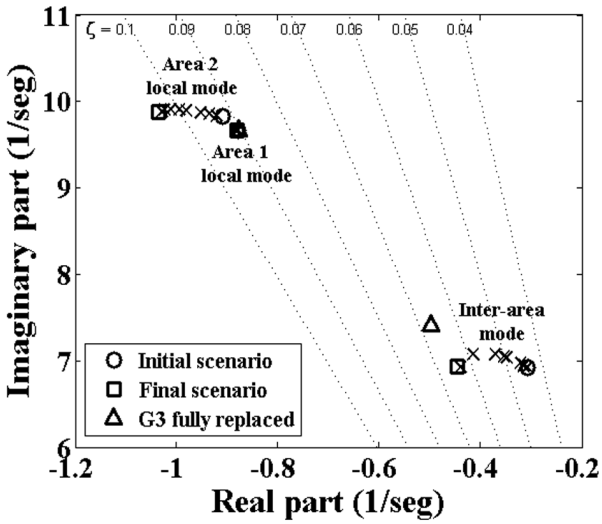

Figure 7. Root loci: Movement of OMs when G3 generation was replaced by wind power generation

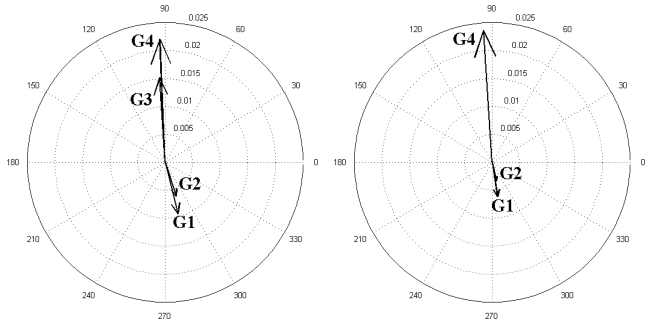

a) b)

Figure 8. Speed mode shape for inter-area mode: a) Initial scenario, and b) Final scenario

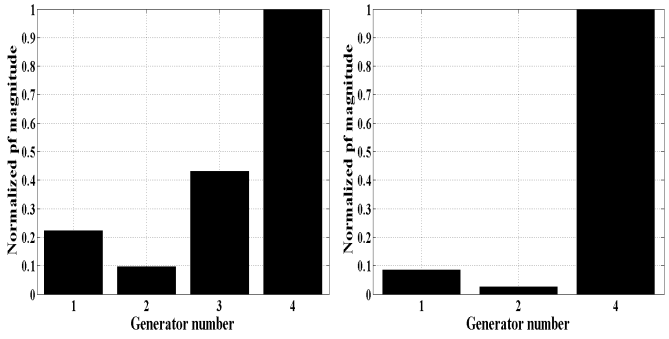

a) b)

Figure 9. Normalized speed participation factors for inter-area mode: a) Initial scenario, and b) Final scenario

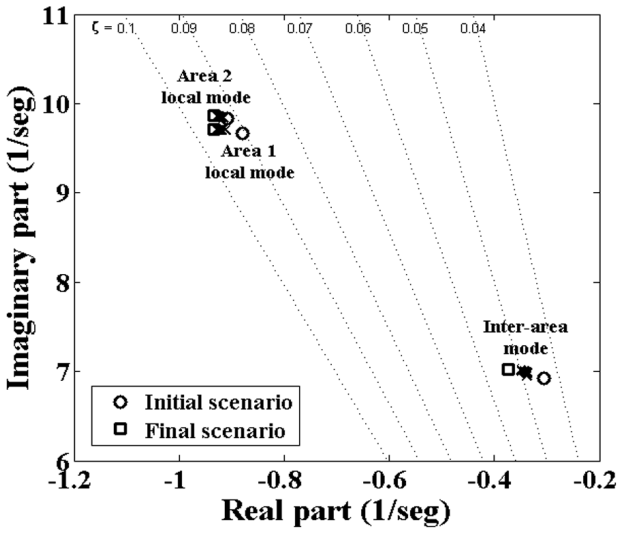

Figure 10. Root loci: Movement of OMs when G2 and G3 generation was replaced by wind power generation

Case3

In Case 3, G3 and G4 generation was replaced gradually by wind generation. Fig. 11 shows the root loci for the three OMs. The circle markers represent the initial scenario and the square markers the final scenario (50 % of G3 and G4 generation replaced by wind generation). It is possible to note that the local modes are not significantly affected. The inter-area mode exhibits a small decrease of damping. This decrease is more noticeable in the final scenario, which corresponds to a more stressed condition (a higher power amount is transferred from Area 1 to Area 2, since power generation from units near loads (G3 and G4) is replaced by wind power generation located far from loads. Thus, the wind power plant appears to contribute to damping decrease when increasing wind power generation contributes in increasing the power system stress level.

Time domain simulations

Time domain simulations were carried out considering a 150 ms self-clearing tree phase fault that is applied at bus 3, for the initial scenario (with low wind power generation) and the final scenario (with high wind power generation) of different cases. Fig. 12 and Fig. 13 show the change in the power angle between G1 and G4 for Case 2 and Case 3, respectively. The initial scenario corresponds to the curves with solid lines and the final scenario corresponds to the curves with dotted lines in each case. As shown in Fig. 12, by observing the first swing, it is clearly evident that the DFG based wind power plant reduces the magnitude of the maximum power angle deviation in Case 2. Thus, the transient stability of the power system has been improved, probably due to the contribution of the wind power plant to reduce the system stress level. Moreover, the inter-area mode is clearly visible as the simulation progress. Comparing both the initial and final scenarios it is interesting to note a small damping increase on inter-area oscillation in the simulation period. These results correlate well with those of linearization-based eigenanalysis. On the other hand, as shown in Fig. 13, the magnitude of the maximum power angle deviation increases in Case 3 (due to the increment of power system stress level). Hence, the transient stability of the power system has worsened. Furthermore, the figure also shows a small damping decrease for the inter-area oscillation, thus confirming the results obtained via linearization-based eigenanalysis.

B. WHT system

The WHT system consists of three strongly meshed areas, 75 buses, 16 conventional power plants, 2 wind power plants, 33 transformers and 73 transmission lines. The transmission lines interconnecting the areas are weak because the length of the lines is about 290 km. Thus, this system is useful to study different kinds of stability problems, especially inter-area oscillations and has been developed based on characteristic parameters of the European power system [20]. The single-line diagram of the system is shown in Fig. 14. The system generating park includes hydro, nuclear, and thermal conventional power plants as well as wind power plants. The total system-wide installed capacity is about 19 GW, of which 1.5 GW correspond to two DFG-based wind power plants. The transmission network comprises the voltage levels 380 kV, 220 kV, and 110 kV.

All synchronous generators are represented using fifth order models extended by IEEE type exciter and governor models [20]. For hydro, thermal, and nuclear generators, the rated power is 220 MVA, 247 MVA, and 259 MVA, respectively. The nominal output power of each wind power plant is 750 MVA. This corresponds to the output of 150 DFIG-based wind generators, each with a nominal capacity of about 5 MVA. Again, a single equivalent model was used to

represent all individual units within each wind power plant that is connected to the system using the layout depicted in Fig. 6.

Deterministic assessment

The intent of this subsection is to ascertain if the indicative findings of the study in the previous subsection are confirmed by large scale prospective analysis. Therefore, sensitive analysis of two cases was carried out: 1) Wind power plant connected to bus 41 (Area C); wind generation gradually replaces generation from conventional power plants within the same area while keeping unaltered the power transfers between areas. 2) Wind power plant connected to bus 17 (Area B); the generation from conventional power plants in Area C is gradually replaced by wind generation located far away (replacing up to 10 percent of the total conventional generation of Area C).

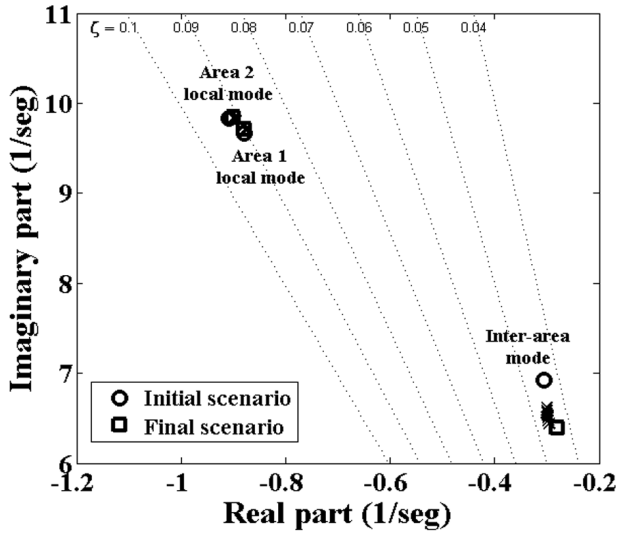

Figure 11. Root loci: Movement of OMs when G3 and G4 generation was replaced by wind power generation

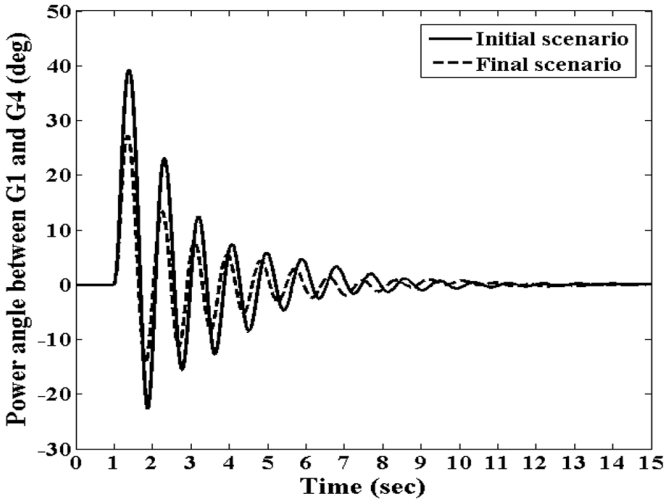

Figure 12. Power angle between G1 and G4 – Case 2

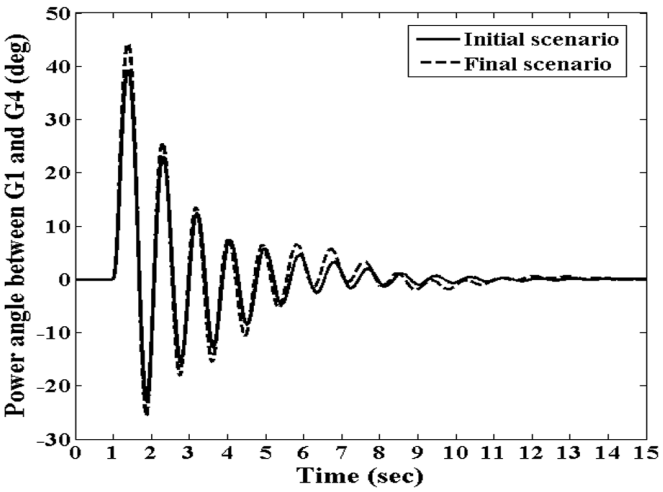

Figure 13. Power angle between G1 and G4 – Case 3

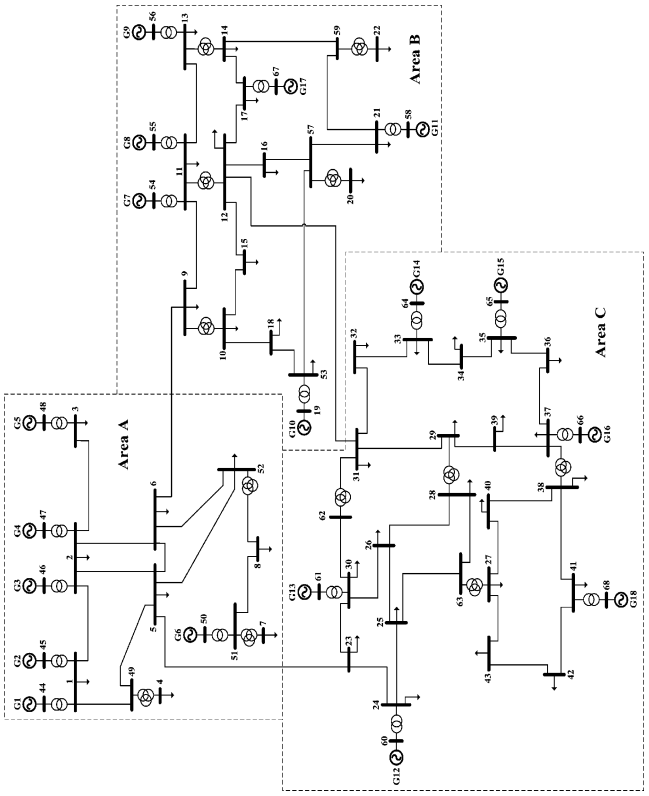

Figure 14. Single-line diagram of the WHT system.

From linearization-based eigenanalysis, two critical modes have been recognized: The first one is an inter-area mode in which the generators in Area A oscillate against those in Area B. The second mode is a control mode associated with the excitation control of the synchronous generators (the largest participation factors correspond to the AVR amplifier states at the generators in Area A).

For the first case, Fig. 15 shows the movement of the critical OMs on the complex plane. The circle markers

represent the initial scenario and the square markers the final scenario (wind power generation replacing up to 10 percent of the total conventional generation of Area C). It is noted that the control mode is not affected whereas the damping of the inter-area mode is somewhat improved. For the second case, the root loci depicted in Fig. 16 shows that there is a minor effect on the damping of the control mode while there is degradation in the damping of the inter-area mode. This is reasonable since reduction of conventional generation in Area C, combined with the introduction of high levels of wind generation, have resulted in greater network congestion, especially in the tie line lines, and this in turn leads to damping degradation. Finally, it should be pointed out that, regarding the inter-area mode, the findings derived from this survey corroborate those of previous subsection.

Probabilistic assessment

Wind power plants connected to buses 17 (area B) and 41 (area B) are considered. The parameters of the multivariate normal probability distribution function (PDF) describing load uncertainties and the discrete PDFs describing the change of generation units' dispatch are derived from those given in [21]. Overall CPU time for probabilistic eigenanalysis with 21040 trials is 6.72 h. Fig. 17 shows a scatter plot with the values of wind power percentage of electricity supply (i.e. penetration level) in the horizontal and vertical axes, respectively. In the figure, each point (which is associated to different scenarios) is depicted in different colors, grey and black, that correspond to values of the damping ratio of the inter-area mode higher and lesser than the 5 % threshold, respectively. Note that there are clouds of points arranged in a discrete manner due to the discrete increase of wind power penetration levels in both areas, which are sampled according to the discrete PDFs that model wind power plant output power. Besides, each cloud represents a set of scenarios with the same wind power percentage of electricity supply but with different samples of nodal load demands and synchronous generator output power. For each cloud, it can be seen that there are scenarios exhibiting inter-area mode damping ratio higher and lesser than the threshold value. Remarkably, observe that the number of black points (i.e. scenarios in which the inter-area mode damping ratio is below the threshold) within each cloud increases as wind power percentages of electricity supply increase in both areas. This is reasonable since the introduction of high levels of wind generation led to considerable changes in network power flows resulting in higher power exchanges between the areas (which entails greater network congestion) and in lesser synchronous generators supplying the grid in response to the high load demand in area C (which decreases the inertia of the system). These observations match with the conclusions reached in the previous subsections. Furthermore, it is worth to mention that other factors (e.g. interactions among controllers) influencing the damping of inter-area modes should be also investigated. This is, however, beyond the scope of this paper.

The values for the R_{Inst} index related to the inter-area mode are presented in Table I, comparing the results of probabilistic eigenanalysis for the baseline system configuration (i.e. without outages) with those considering the outage of G17 wind power plant and the addition of a PSS at G11 according to the mean of the participation factors associated with the generator speed deviation states ($\Delta\omega$). Note also that the outage of G17 wind power plant increases the instability risk due to poorly damped inter-area oscillations, most likely because it causes higher power transfers from areas A and B to area C, thus exacerbating the network congestion. Besides, these results indicate that a properly located PSS will improve the effectiveness of the PSS in enhancing the damping of the inter-area mode for the baseline system configuration, whereas, by contrast, it can be seen that although the addition of the PSS helps in significantly decreasing the instability risk, more countermeasures are required to ensure well damped inter-area oscillations over the whole set of operating conditions.

IV. CONCLUSIONS

In this paper, a survey of the impact of large scale wind power integration on power system small signal-stability is thoroughly discussed. For this purpose, different factors concerning wind power generation such as wind power integration levels and wind power plant location are considered in the small signal stability assessment of two benchmark power systems via linearization-based eigenanalysis, probabilistic eigenanalysis and time domain simulations. For both systems, it was found out that large wind power integration can have a positive or negative impact on the damping of inter-area oscillations. The impact depends on the location of the wind power plant, the amount of the conventional generation replaced by wind power and the degree of network congestion. Remarkably, in the TAFM system, changes in the shape of Area 2 local mode and the inter-area mode arose when a synchronous generator involved in these oscillatory modes was fully replaced by the wind power plant within the same area. Additionally, it appeared that wind power does not affect local oscillations in distant areas. Furthermore, these factors should be accounted in PSS tuning and in the definition of additional countermeasures since the structure of power system oscillations can suffer modifications.

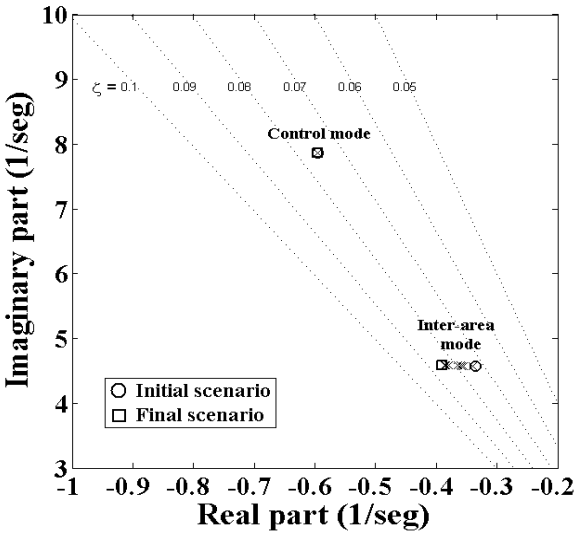

Figure 15. Movement of critical OMs – First case

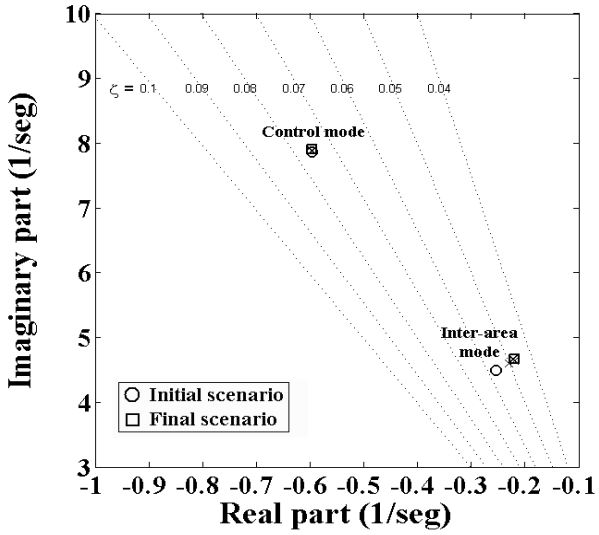

Figure 16. Movement of critical OMs – Second case

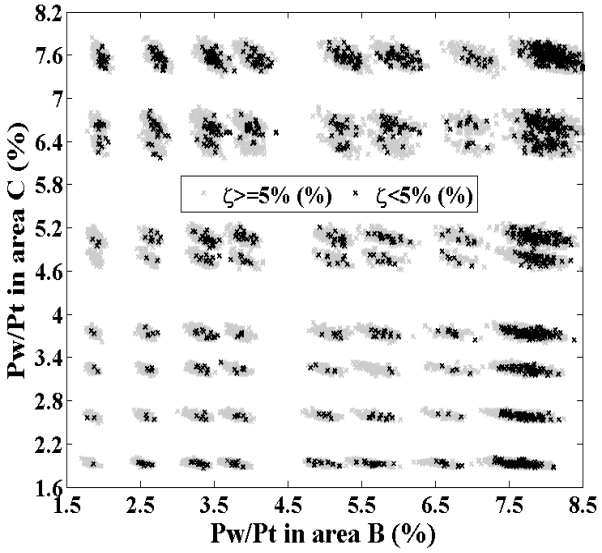

Figure 17. The effect of wind generation on the inter-area mode damping ratio. Pw/Pt denotes the ratio of the wind power delivered divided by the total power delivered

TABLE I. INTER-AREA MODE - R_{INST} INDEX

R_{Inst} / Config.	Baseline		Outage of G17	
	Without PSS	With PSS	Without PSS	With PSS
$OM_{\zeta\text{-Neg}}$	0.0000	0.0000	0.0000	0.0000
$OM_{\zeta\text{-Poor}}$	0.0750	0.0000	0.0841	0.0076
$OM_{\zeta\text{-Damp}}$	0.9250	1.0000	0.9159	0.9924

REFERENCES

[1] Erlich, and F. Shewarega, "Interaction of large wind power generation plants with the power system," IEEE International Power and Energy Conference, pp. 12 - 18, Nov. 2006.

[2] R. Thresher, M. Robinson, and P. Veers, "To capture the wind," IEEE Power and Energy Magazine, Vol. 5, No. 6, pp. 34 - 46, Nov.-Dec. 2007.

[3] J.C. Smith, , and B. Parsons, "What does 20% look like?," IEEE Power and Energy Magazine, Vol. 5, No. 6, pp. 22 – 33, Nov.-Dec. 2007.

[4] I. Erlich, and F. Shewarega, "Introduction of wind power generation into the first course in power systems," IEEE Power Engineering Society General Meeting, pp. 1 – 8, June 2007.

[5] J. G. Slootweg, "Wind power: Modelling and impact on power system dynamics," Ph.D Thesis, Technische Universiteit Delft, 2003.

[6] F. Wu, X.-P. Zhang, K. Godfrey, and P. Ju, "Small signal stability analysis and optimal control of a wind turbine with doubly fed induction generator," IET Generation, Transmission & Distribution, Vol. 1, No. 5, pp. 751 – 760, Sep. 2007.

[7] S. Muller, M. Deicke, and R.W. De Doncker, "Doubly fed induction generator systems for wind turbines," IEEE Industry Applications Magazine, Vol. 8, No. 3, pp. 26 – 33, May-June 2002.

[8] F. Shewarega, I. Erlich, and J.L. Rueda, "Impact of large offshore wind farms on power system transient stability," IEEE/PES Power Systems Conference and Exposition, pp. 1-8, March 2009.

[9] T. Ackermann, Wind Power in Power Systems. West Sussex: John Wiley & Sons, 2005.

[10] P. Rosas, "Dynamic influences of wind power on the power system," Ph.D Thesis, Technical University of Denmark., March 2003.

[11] V. Akhmatov, "Analysis of dynamic behaviour of electric power systems with large amount of wind power," Ph.D Thesis, Technical University of Denmark, April 2003.

[12] A. Mendonca, and J.A.P. Lopes, "Impact of large scale wind power integration on small signal stability," International Conference on Future Power Systems, pp. 1 – 5, Nov. 2005.

[13] D.J. Vowles, C. Samarasinghe, M.J. Gibbard, and G. Ancell, "Effect of wind generation on small-signal stability — A New Zealand example", IEEE Power and Energy Society General Meeting - Conversion and Delivery of Electrical Energy in the 21st Century, pp. 1 – 8, July 2008.

[14] L. L. Grigsby, Power system stability and control. Boca Raton: Taylor & Francis Group, 2007.

[15] J. L. Rueda, D. G. Colomé, and I. Erlich, "Assessment and enhancement of small signal stability considering uncertainties," IEEE Transactions on Power Systems, Vol. 24, No. 1, pp. 198-207, Feb. 2009.

[16] I. Erlich, J. Kretschmann, J. Fortmann, S. Mueller-Engelhardt, and H. Wrede, "Modeling of wind turbines based on doubly-fed induction generators for power system stability studies," IEEE Transactions on Power Systems, Vol. 22, No. 3, pp. 909 – 919, Aug. 2007.

[17] P. Kundur, Power System Stability and Control. New York: Mc.Graw-Hill, 1994.

[18] M. Pöller, and S. Achilles, "Aggregated wind park models for analyzing power system dynamics," [Online]. Available: http://www.digsilent.de/Consulting/Publications

[19] I. Erlich, "Analysis and simulation of the dynamic behavior of electrical power systems," Postdoctoral lecture qualification, Department of Electrical Engineering, Dresden University, Germany, 1995.

[20] S. P. Teeuwsen, I. Erlich, and M. A. El-Sharkawi, "Neural network based classification method for small-signal stability assessment," IEEE Bologna Power Tech Conference Proceedings, Vol. 3, pp. 1 – 6, June 2003.

[21] J. L. Rueda, and D. G. Colomé, "Probabilistic performance indexes for small signal stability enhancement in weak wind-hydro-thermal power systems", IET Generation, Transmission & Distribution Journal, Vol. 3, No. 8, pp. 733 – 747, Aug. 2009.